Computers & Fluids 100 (2014) 227–236

Contents lists available at ScienceDirect

Computers & Fluids

journal homepage: www.elsevier.com/locate/compfluid

Analyze of fluid flow and heat transfer of nanofluids over a stretching sheet near the extrusion slit

Aminreza Noghrehabadi *, Ehsan Izadpanahi, Mohammad Ghalambaz

Department of Mechanical Engineering, Shahid Chamran University of Ahvaz, Ahvaz, Iran

ARTICLE INFO

Article history:
Received 3 November 2013
Received in revised form 18 April 2014
Accepted 13 May 2014
Available online 22 May 2014

Keywords:
Stretching sheet
Extrusion slit
Finite difference
Nanofluid
Brownian motion
Thermophoresis
Variable thermal conductivity

ABSTRACT

The objective of the present study is to analyze the boundary layer flow and heat transfer of nanofluids over a stretching sheet near the extrusion slit in the presence of variable thermal conductivity. The effects of Brownian motion and thermophoresis are taken into account. The governing partial differential equations are reduced to dimensionless form and solved numerically using finite difference scheme and Point Successive Over Relaxation algorithm. The critical Reynolds number is introduced to distinguish the non-similar region from the self-similar region of velocity and temperature profiles. Furthermore, the effects of dimensionless parameters such as Prandlt number, Schmidt number, variable thermal conductivity parameter, Brownian motion and thermophoresis parameters on the velocity and temperature profiles and also on reduced Nusselt number, reduced Sherwood number and critical Reynolds number are investigated. It is found that the critical Reynolds number for the temperature profile is significantly affected by Prandtl number. In addition, the reduced Nusselt and Sherwood numbers found to be much higher in non-similar regions near the extrusion slit than that of self-similar region.

1. Introduction

Fluid flow and heat transfer in a boundary layer flow over a stretching sheet has been studied by many researchers; because it has significant applications in many industries such as extrusion of plastic, paper production, metal spinning, wire drawing, glass blowing, hot rolling, manufacture of rubber sheet, polymer engineering, cooling of metallic sheets and crystal growing [1,2].

Sakiadis [3,4] examined viscous flow over a continuous solid surface with application of boundary layer theory. Crane [5] was the first one who extended the work of Sakiadis [3,4] and studied the viscous flow and heat transfer caused by a linearly stretching sheet. After pioneer work by Crane [5], Al-Sanea and Ali [6] studied flow and heat-transfer over a continuously moving horizontal material in the presence of suction or injection very close and far away downstream from the extrusion slit. They are considered the effects of extrusion slit by solving the governing partial differential equations used finite volume method and carried out the solutions in the non-similar and similar regions. Further, Kiwan and Ali [7] did the same case for the flow and heat transfer over a stretching surface in a porous medium with internal heat generation or absorption and suction and injection. They considered full governing equations for mapping out the solution near the slit and far away downstream from the extrusion slit.

The heat transfer rate from the sheet is very important in such application because it induces a direct impact on the quality of the products. However, the common heat transfer fluids such as water, ethylene glycol, and engine oil have limited heat transfer capabilities owing to their low thermal conductivity whereas metals have much higher thermal conductivities than these fluids. Therefore, dispersing high thermal conductive solid particles in a conventional heat transfer fluid may enhance the thermal conductivity of the resulting fluid.

Nanofluid is a fluid containing nanometer-sized particles. The term "Nanofluid" was proposed by Choi [8] to indicate engineered colloids consist of nanoparticles dispersed in a base fluid. The base fluid is usually a conductive fluid, such as water or ethylene glycol. Other base fluids include bio-fluids, polymer solutions, oils and other lubricants. The nanoparticles used in synthesis of nanofluids are typically metallic (Al, Cu), metallic oxides (Al_2O_3, TiO_2), carbides (SiC), nitrides (AlN, SiN) or carbon nanotubes with the diameter which ranges between 1 and 100 nm. One of the outstanding characteristic of nanofluids is their enhanced thermal conductivity [9]. Comprehensive references on this subject can be found in the recently published book by Das et al. [10] and in the papers by

* Corresponding author. Tel.: +98 611 3330010x5678; fax: +98 611 3336642.
E-mail addresses: noghrehabadi@scu.ac.ir (A. Noghrehabadi), ehsan.izadpanahi@yahoo.com (E. Izadpanahi), m.ghalambaz@gmail.com (M. Ghalambaz).

http://dx.doi.org/10.1016/j.compfluid.2014.05.013
0045-7930/

Nomenclature

a	constant
C	nanoparticle volume fraction
C_w	nanoparticle volume fraction at the stretching sheet
C_∞	ambient nanoparticle volume fraction
C_f	skin friction coefficient
D_B	Brownian diffusion coefficient
D_T	thermophoresis diffusion coefficient
H	height normal to the sheet
k	thermal conductivity
$k_{m,\infty}$	the effective thermal conductivity of the nanofluid outside the boundary layer
L	length of the sheet
m_w	wall mass flux
Nb	Brownian motion parameter
Nc	variable thermal conductivity parameter
Nt	thermophoresis parameter
Nu	Nusselt number
P	pressure
Pr	Prandtl number
q_w	wall Heat flux
Re_L	Reynolds number
Sc	Schmidt number
Sh	Sherwood number
T	fluid temperature
T_∞	ambient temperature
T_w	temperature at the stretching sheet
u,v	velocity components along x and y-axes
u_w	velocity of the stretching sheet
x, y	physical coordinates (x-axis is aligned along the stretching sheet and y-axis is normal to it)

Greek

α	thermal diffusivity
β	clustering parameter
$\varphi(\eta)$	dimensionless nanoparticle volume fraction
η	similarity variable
$\theta(\eta)$	dimensionless temperature
υ	kinematic viscosity of nanofluid
$(\rho c)_{nf}$	heat capacity of the nanofluid
$(\rho c)_{\mathrm{p}}$	effective heat capacity of the nanoparticle material
ρ	nanofluid density
ρ_p	nanoparticle mass density
ψ	stream function
ω	vorticity function
ξ, ζ	computational coordinates (ξ-axis is aligned along the stretching sheet and ζ-axis is normal to it)

Superscript

*	dimensional parameters

Subscript

C	critical value
CFD	PSOR result
nf	nanofluid
p	nanoparticles
sim	similarity result
∞	ambient value

Wang and Mujumdar [11], Kakaç and Pramuanjaroenkij [12], Chandrasekar et al. [13] and Wu and Zhao [14].

The effects of nanofluids could be considering in different ways such as dynamic effects which include the effects of Brownian motion and thermophoresis diffusion [15–17], and the static part of Maxwell's theory [18–21].

Recently, many researchers, using similarity solution, have examined the boundary layer flow, heat and mass transfer of nanofluids over stretching sheets. Khan and Pop [22] have analyzed the boundary-layer flow of a nanofluid past a stretching sheet using a model in which the Brownian motion and thermophoresis effects were taken into account. They reduced the whole governing partial differential equations into a set of nonlinear ordinary differential equations and solved them numerically. In addition, the set of ordinary differential equations which was obtained by Khan and Pop [22] has been solved by Hassani et al. [23] using homotopy analysis method. After that, many researchers, using similarity solution approach, have extended the heat transfer of nanofluids over stretching sheets and examined the other effects such as the chemical reaction and heat radiation [24], convective boundary condition [25], nonlinear stretching velocity [26], partial slip boundary condition [27],magnetic nanofluid [28], partial slip and convective boundary condition [29], heat generation/absorption [30], thermal and solutal slip [31], nano non-Newtonian fluid [32], and Oldroyd-B Nanofluid [33]. In all of the mentioned studies [22–33], it was assumed that the values of the Reynolds number are high and the effects of extrusion slit could be neglected, because of that, the similarity solution were used to carried out the results. However, the analysis of the boundary layer of regular fluids over stretching sheets reveals that for the low values of the Reynolds number, the boundary layer approximations are not valid in the vicinity of the slit; hence, the extrusion slit significantly affects the boundary layer flow and heat transfer [6,7]. In addition, the stretching velocity of the sheet is very low in many practical applications; and hence, the practical Reynolds number is also very low. At the present time, it is not clear when the boundary layer approximations are adequate for analysis of flow and heat transfer of nanofluids over a stretching sheet in the case of flow and heat transfer of nanofluids.

As mentioned, the enhancement of the thermal conductivity of nanofluids is the most outstanding thermo-physical properties of nanofluids. In all of the previous studies [22–33], the effect of local volume fraction of nanoparticles on the thermal conductivity of the nanofluid was neglected [34,35]. However, in the work of Buongiorno [36], it has been reported that the local concentration of nanoparticles may significantly affect the local thermal conductivity of the nanofluids.

The objective of the present study is to analyze the flow and heat transfer of nanofluids near the extrusion slit and where the Reynolds number of the flow is low. The effect of local volume fraction of nanoparticles on the thermal conductivity of nanofluid is taken into account. A critical Reynolds number, $Re_{L,C}$, is introduced to distinguish between the self-similar and non-similar regions of the velocity and temperature profiles. The results of present study also provide practical guidelines for the adequately of the available similarity solutions.

2. Formulation of the problem

Consider the two dimensional laminar steady flow of an incompressible nanofluid caused by stretching of the sheet, where the x^*-axis is measured along the sheet and the y^*-axis is measured normal to the sheet (see Fig. 1). It is assumed that the temperature (T^*) and the nanoparticles volume fraction (C^*) are constant at the

surface. The temperature of sheet and volume fraction of nanoparticles on the surface is denoted by T_w^* and C_w^*, respectively. The temperature and volume fraction of nanoparticles outside the boundary layer (ambient) is denoted by T_∞^* and C_∞^*, respectively. Following the work of Buongiorno [36] and Khan and Pop [22], the basic steady state equations for the conservation nanofluid, momentum, thermal energy and conservation of nanoparticles are written as:

$$\frac{\partial u^*}{\partial x^*}+\frac{\partial v^*}{\partial y^*}=0 \tag{1}$$

$$u^*\frac{\partial u^*}{\partial x^*}+v^*\frac{\partial u^*}{\partial y^*}+\frac{1}{\rho}\frac{\partial P^*}{\partial x^*}=\upsilon\left(\frac{\partial^2 u^*}{\partial x^{*2}}+\frac{\partial^2 u^*}{\partial y^{*2}}\right) \tag{2}$$

$$u^*\frac{\partial v^*}{\partial x^*}+v^*\frac{\partial v^*}{\partial y^*}+\frac{1}{\rho}\frac{\partial P^*}{\partial y^*}=\upsilon\left(\frac{\partial^2 v^*}{\partial x^{*2}}+\frac{\partial^2 v^*}{\partial y^{*2}}\right) \tag{3}$$

$$u^*\frac{\partial T^*}{\partial x^*}+v^*\frac{\partial T^*}{\partial y^*}=\frac{1}{(\rho c)_{nf}}\nabla.[k_m(C^*)\nabla.T^*]+\frac{(\rho c)_p}{(\rho c)_{nf}}\left\{D_B\left(\frac{\partial T^*}{\partial x^*}\frac{\partial C^*}{\partial x^*}+\frac{\partial T^*}{\partial y^*}\frac{\partial C^*}{\partial y^*}\right)+\frac{D_T}{T_\infty^*}\left[\left(\frac{\partial T^*}{\partial x^*}\right)^2+\left(\frac{\partial T^*}{\partial y^*}\right)^2\right]\right\} \tag{4}$$

$$u^*\frac{\partial C^*}{\partial x^*}+v^*\frac{\partial C^*}{\partial y^*}=D_B\left(\frac{\partial^2 C^*}{\partial x^{*2}}+\frac{\partial^2 C^*}{\partial y^{*2}}\right)+\frac{D_T}{T_\infty^*}\left\{\frac{\partial^2 T^*}{\partial x^{*2}}+\frac{\partial^2 T^*}{\partial y^{*2}}\right\} \tag{5}$$

The boundary conditions at the extrusion slit, surface of the sheet, out flow and far from the sheet are respectively written as:

$$u^*=0,\quad v^*=0,\quad T^*=T_\infty^*,\quad C^*=C_\infty^*\quad \text{at}:\ x^*=0 \tag{6}$$

$$u^*=u_W^*=ax^*,\quad v^*=0,\quad T^*=T_W^*,\quad C^*=C_W^*\quad \text{at}:\ y^*=0 \tag{7}$$

$$\frac{\partial u^*}{\partial x^*}=0,\quad \frac{\partial v^*}{\partial x^*}=0,\quad \frac{\partial T^*}{\partial x^*}=0,\quad \frac{\partial C^*}{\partial x^*}=0\quad \text{at}:\ x^*=L \tag{8}$$

$$u^*=0,\quad \frac{\partial v^*}{\partial y^*}=0,\quad T^*=T_\infty^*,\quad C=C_\infty^*\quad \text{at}:\ y^*=H \tag{9}$$

Here, u^* and v^* are the velocity components along the x^* axis and y^* axis, respectively. T^* is the temperature, C^* is the volume fraction of nanoparticles, P^* is the fluid pressure, ρ is the density of the nanofluid, υ is the kinematic viscosity of the nanofluid, D_B is the Brownian diffusion coefficient, D_T is the thermophoresis diffusion coefficient, $(\rho c)_p$ is the effective heat capacity of the nanoparticles, $(\rho c)_{nf}$ is the heat capacity of the nanofluid and $k_m(C^*)$ is the thermal conductivity. The thermal conductivity is assumed as a linear function of nanoparticles volume fraction as follow:

$$k_m(C^*)=k_{m,\infty}\left(1+Nc\frac{(C^*-C_\infty^*)}{C_w^*-C_\infty^*}\right) \tag{10}$$

where $k_{m,\infty}$ is the thermal conductivity of the nanofluid outside the boundary layer and Nc denotes the variable thermal conductivity parameter. Nc is function of C_∞^* and the thermal conductivity of nanofluid. However, Nc can be assumed constant for a specified type of nanofluid and fixed value of ambient volume fraction. In order to perform a general non-dimensional analysis, Eqs. (1)–(9) are written in the non-dimensional form using the following non-dimensional parameters:

$$x=\frac{x^*}{L},\quad y=\frac{y^*}{L} \tag{11}$$

$$u=\frac{u^*}{u_L},\quad v=\frac{v^*}{u_L},\quad P=\frac{P^*}{\rho u_L^2} \tag{12}$$

$$T=\frac{T^*-T_\infty^*}{T_W^*-T_\infty^*},\quad C=\frac{C^*-C_\infty^*}{C_W^*-C_\infty^*} \tag{13}$$

Introducing stream (ψ) and vorticity (ω) functions, the pressure terms can be eliminated from the momentum equations.

$$\omega=\frac{\partial v}{\partial x}-\frac{\partial u}{\partial y} \tag{14}$$

$$u=\frac{\partial \psi}{\partial y},\quad v=-\frac{\partial \psi}{\partial x} \tag{15}$$

Now, using Eqs. (10)–(15), the non-dimensional form of the governing equations, Eqs. (1)–(5), is obtained as follows:

$$-\omega=\frac{\partial^2\psi}{\partial x^2}+\frac{\partial^2\psi}{\partial y^2} \tag{16}$$

$$u\frac{\partial \omega}{\partial x}+v\frac{\partial \omega}{\partial y}=\frac{1}{Re_L}\left(\frac{\partial^2\omega}{\partial x^2}+\frac{\partial^2\omega}{\partial y^2}\right) \tag{17}$$

$$Re_L\left(u\frac{\partial T}{\partial x}+v\frac{\partial T}{\partial y}\right)=\frac{1+Nc.C}{Pr}\left(\frac{\partial^2 T}{\partial x^2}+\frac{\partial^2 T}{\partial y^2}\right)+\left(\frac{Nc}{Pr}+Nb\right)\left\{\left(\frac{\partial T}{\partial x}\frac{\partial C}{\partial x}\right)+\left(\frac{\partial T}{\partial y}\frac{\partial C}{\partial y}\right)\right\}+Nt\left\{\left(\frac{\partial T}{\partial x}\right)^2+\left(\frac{\partial T}{\partial y}\right)^2\right\} \tag{18}$$

$$Re_L Sc\left(u\frac{\partial C}{\partial x}+v\frac{\partial C}{\partial y}\right)=\left(\frac{\partial^2 C}{\partial x^2}+\frac{\partial^2 C}{\partial y^2}\right)+\frac{Nt}{Nb}\left\{\frac{\partial^2 T}{\partial x^2}+\frac{\partial^2 T}{\partial y^2}\right\} \tag{19}$$

Similarly, the non-dimensional boundary conditions are obtained as follows:

$$\psi=0,\quad \omega=-\frac{\partial^2\psi}{\partial x^2},\quad T=0,\quad C=0\quad \text{at}:\ x=0 \tag{20}$$

$$\frac{\partial\psi}{\partial y}=x,\quad \omega=-\frac{\partial^2\psi}{\partial y^2},\quad T=1,\quad C=1\quad \text{at}:\ y=0 \tag{21}$$

$$\frac{\partial^2\psi}{\partial x^2}=0,\quad \frac{\partial\omega}{\partial x}=0,\quad \frac{\partial T}{\partial x}=0,\quad \frac{\partial C}{\partial x}=0\quad \text{at}:\ x=1 \tag{22}$$

$$\frac{\partial\psi}{\partial y}=0,\quad \omega=-\frac{\partial^2\psi}{\partial x^2},\quad T=0,\quad C=0\quad \text{at}:\ y=\frac{H}{L} \tag{23}$$

where the parameters of Re_L, Pr, Sc, Nb and Nt are defined as:

$$Re_L=\frac{aL^2}{\upsilon},\quad \alpha_m=\frac{k_{m,\infty}}{(\rho c)_{nf}},\quad Pr=\frac{\upsilon}{\alpha_m},\quad \mathrm{Sc}=\frac{\upsilon}{D_B} \tag{24}$$

$$Nb=\frac{(\rho c)_p D_B(C_W^*-C_\infty^*)}{(\rho c)_{nf}\upsilon},\quad Nt=\frac{(\rho c)_p D_T(T_W^*-T_\infty^*)}{(\rho c)_{nf}\upsilon T_\infty^*} \tag{25}$$

Here, Re_L, Pr, Sc, Nb and Nt denote the Reynolds number, Prandtl number, Schmidt number, Brownian motion parameter and thermophoresis parameter, respectively.

In the similarity solution approach [22–31], the Reynolds number Re_L, presents in Eqs. (17)–(19), is eliminated by introducing the similarity variable, $\eta=(a/\upsilon)^{1/2}y^*$, that leads to neglecting the effects of extrusion slit. In order to consider the effects of extrusion slit, the full governing partial differential equations, Eqs. (16)–(19), should be solved and then the results for the velocity, temperature and concentration profile can be changed to the similarity coordinates by using the following equations:

$$\eta = y(Re_L)^{\frac{1}{2}}, \quad f'(\eta) = \frac{u(x,y)}{x}, \quad \theta(\eta) = T(x,y), \quad \phi(\eta) = C(x,y) \tag{26}$$

The important non-dimensional parameters of heat and mass transfer, the quantities of the skin friction coefficient, Nusselt number and Sherwood number, are introduced as follow:

$$C_{fx} = \frac{\mu_{nf}\frac{\partial u^*}{\partial y^*}|_{y^*=0}}{\frac{1}{2}\rho_{nf}u_w^{*2}}, \quad Nu = \frac{x^* q_w}{k(T_W^* - T_\infty^*)}, \quad Sh = \frac{x^* m_w}{D_B(C_W^* - C_\infty^*)} \tag{27}$$

where q_w is the wall heat flux and m_w is the wall mass flux. Using dimensionless parameters, Eqs. (11)–(13), and the definition of the values q_w ($q_w = -k\partial T^*/\partial y^*$) and m_w ($m_w = -D_B\partial C^*/\partial y^*$), Eq. (27) become,

$$C_{fx} = \frac{2}{u_w^2 Re_L}\frac{\partial u}{\partial y}\bigg|_{y=0}, \quad Nu = -x\frac{\partial T}{\partial y}, \quad Sh = -x\frac{\partial C}{\partial y} \tag{28}$$

The reduced skin friction coefficient, Nusselt and Sherwood numbers are introduced as follows:

$$Cfr = 2xu_w^{-2}Re_L^{-\frac{1}{2}}\frac{\partial u}{\partial y}\bigg|_{y=0}, \quad Nur = -\frac{1}{\sqrt{Re_L}}\frac{\partial T}{\partial y}, \quad Shr = -\frac{1}{\sqrt{Re_L}}\frac{\partial C}{\partial y} \tag{29}$$

For estimating the valid self-similar region, the results of the present study should be compared with the results of the similarity solution. The following equation is used to compute errors between the results of similarity solution which belongs to the self-similar region and CFD results that relate to the solution of partial differential equations.

$$error = \max\left(\left|\frac{\chi_{sim} - \chi_{CFD}}{\chi_{sim,\max}}\right|\right)\Bigg|_{j=1}^{n} \times 100 \tag{30}$$

where χ is u, T or C for the momentum equation, energy equation or concentration equation respectively. χ also can be *Nur* for the reduced Nusselt number and *Shr* for the reduced Sherwood number. The subscript of *sim* indicates the solution obtained by similarity approach and *CFD* indicates the computational fluid dynamic solution.

3. Grid generation and numerical method

In the boundary layer flows, which include large gradients in a specific region, additional resolution of the flow properties is necessary. Likewise, there are large gradients which are centralized near the surface of the sheet and near the extrusion slit; thus, an accurate computation requires a large number of grid points. Therefore, grid points can be clustered in the region of high gradients rather than using a uniform grid points distributed in the physical domain. Clustering the grid points would significantly reduce the total number of required grid points and thus boost the efficiency and accuracy of the numerical approach. The simplest grid generation technique, that is capable of generating the non-uniform grid point, is the algebraic method. The major benefit of this scheme is the speed in which a grid can be generated. In the algebraic method, an algebraic equation is needed to relate the grid points in the computational domain to those of the physical domain. The algebraic equations, used in the present study, are introduced as follows:

$$x = L\frac{(\beta_x+1) - (\beta_x-1)\left(\frac{\beta_x+1}{\beta_x-1}\right)^{\left(1-\frac{\xi}{\xi_{MAX}}\right)}}{1 + \left(\frac{\beta_x+1}{\beta_x-1}\right)^{\left(1-\frac{\xi}{\xi_{MAX}}\right)}} \tag{31}$$

$$y = H\frac{(\beta_y+1) - (\beta_y-1)\left(\frac{\beta_y+1}{\beta_y-1}\right)^{\left(1-\frac{\zeta}{\zeta_{MAX}}\right)}}{1 + \left(\frac{\beta_y+1}{\beta_y-1}\right)^{\left(1-\frac{\zeta}{\zeta_{MAX}}\right)}} \tag{32}$$

where β_x and β_y are the clustering parameters in x and y directions, respectively. The ranges of these parameters are between 1 and ∞. More grid points are clustered near the surface of the sheet when the values of β getting close to 1.

The chain rule for partial differentiation yields the following expressions:

$$\frac{\partial}{\partial x} = \xi_x\frac{\partial}{\partial \xi}, \quad \frac{\partial^2}{\partial x^2} = \xi_{xx}\frac{\partial}{\partial \xi} + \xi_x^2\frac{\partial^2}{\partial \xi^2} \tag{33}$$

$$\frac{\partial}{\partial y} = \zeta_y\frac{\partial}{\partial \zeta}, \quad \frac{\partial^2}{\partial y^2} = \zeta_{yy}\frac{\partial}{\partial \zeta} + \zeta_y^2\frac{\partial^2}{\partial \zeta^2} \tag{34}$$

where $\xi_x = \partial\xi/\partial x$, $\xi_{xx} = \partial^2\xi/\partial x^2$ and $\zeta_y = \partial\zeta/\partial y$, $\zeta_{yy} = \partial^2\zeta/\partial y^2$. Because ξ is independent from y and ζ is independent from x, the values of ξ_y, ξ_{yy}, ζ_x and ζ_{xx} are zero. Using Eqs. (31)–(34), the dimensionless governing partial differential equations, Eqs. (16)–(19), are transformed to the computational domain as follows:

$$u\xi_x\frac{\partial\omega}{\partial\xi} + v\zeta_y\frac{\partial\omega}{\partial\zeta} = \frac{1}{Re_L}\left(\xi_x^2\frac{\partial^2\omega}{\partial\xi^2} + \xi_{xx}\frac{\partial\omega}{\partial\xi} + \zeta_y^2\frac{\partial^2\omega}{\partial\zeta^2} + \zeta_{yy}\frac{\partial\omega}{\partial\zeta}\right) \tag{35}$$

$$\omega = -\left(\xi_x^2\frac{\partial^2\psi}{\partial\xi^2} + \xi_{xx}\frac{\partial\psi}{\partial\xi} + \zeta_y^2\frac{\partial^2\psi}{\partial\zeta^2} + \zeta_{yy}\frac{\partial\psi}{\partial\zeta}\right) \tag{36}$$

$$\begin{aligned} Re_L\left(u\xi_x\frac{\partial T}{\partial\xi} + v\zeta_y\frac{\partial T}{\partial\zeta}\right) = {} & \frac{1+Nc.C}{Pr}\left(\xi_x^2\frac{\partial^2 T}{\partial\xi^2} + \xi_{xx}\frac{\partial T}{\partial\xi} + \zeta_y^2\frac{\partial^2 T}{\partial\zeta^2} + \zeta_{yy}\frac{\partial T}{\partial\zeta}\right) \\ & + \left(\frac{Nc}{Pr} + Nb\right)\left\{\left(\xi_x^2\frac{\partial T}{\partial\xi}\frac{\partial C}{\partial\xi}\right) + \left(\zeta_y^2\frac{\partial T}{\partial\zeta}\frac{\partial C}{\partial\zeta}\right)\right\} \\ & + Nt\left\{\left(\xi_x\frac{\partial T}{\partial\xi}\right)^2 + \left(\zeta_y\frac{\partial T}{\partial\zeta}\right)^2\right\} \end{aligned} \tag{37}$$

$$\begin{aligned} Re_L Sc\left(u\xi_x\frac{\partial C}{\partial\xi} + v\zeta_y\frac{\partial C}{\partial\zeta}\right) = {} & \left(\xi_x^2\frac{\partial^2 C}{\partial\xi^2} + \xi_{xx}\frac{\partial C}{\partial\xi} + \zeta_y^2\frac{\partial^2 C}{\partial\zeta^2} + \zeta_{yy}\frac{\partial C}{\partial\zeta}\right) \\ & + \frac{Nt}{Nb}\left\{\xi_x^2\frac{\partial^2 T}{\partial\xi^2} + \xi_{xx}\frac{\partial T}{\partial\xi} + \zeta_y^2\frac{\partial^2 T}{\partial\zeta^2} + \zeta_{yy}\frac{\partial T}{\partial\zeta}\right\} \end{aligned} \tag{38}$$

Likewise, the boundary conditions, Eqs. (20)–(23), are transformed as:

$$\psi = 0, \quad \omega = -\left(\xi_x^2\frac{\partial^2\psi}{\partial\xi^2} + \xi_{xx}\frac{\partial\psi}{\partial\xi}\right), \quad T = 0, \quad C = 0 \quad \text{at}: \ x = 0 \tag{39}$$

$$\zeta_y\frac{\partial\psi}{\partial\zeta} = x, \quad \omega = -\left(\zeta_y^2\frac{\partial^2\psi}{\partial\zeta^2} + \zeta_{yy}\frac{\partial\psi}{\partial\zeta}\right), \quad T = 1, \quad C = 1 \quad \text{at}: \ y = 0 \tag{40}$$

$$\xi_x^2\frac{\partial^2\psi}{\partial\xi^2} + \xi_{xx}\frac{\partial\psi}{\partial\xi} = 0, \quad \frac{\partial\omega}{\partial\xi} = 0, \quad \frac{\partial T}{\partial\xi} = 0, \quad \frac{\partial C}{\partial\xi} = 0 \quad \text{at}: \ x = 1 \tag{41}$$

$$\frac{\partial\psi}{\partial\zeta} = 0, \quad \omega = -\left(\xi_x^2\frac{\partial^2\psi}{\partial\xi^2} + \xi_{xx}\frac{\partial\psi}{\partial\xi}\right), \quad T = 0, \quad C = 0 \quad \text{at}: \ y = \frac{H}{L} \tag{42}$$

In order to execute an accurate computation, the non-dimensional top boundary condition (at H/L) should be located in an appropriate large distance from the surface of the sheet ($y = 0$). It is clear that the location of the non-dimensional top boundary condition depends on the thickness of boundary layer. Considering Eq. (26), the top boundary condition can be approximated by the following relation:

$$\frac{H}{L} = \eta_\infty (Re_L)^{-\frac{1}{2}} \tag{43}$$

where η_∞ is 12.

The transformed non-dimensional equations, Eqs. (35)–(38), subject to the boundary conditions, Eqs. (39)–(42), are numerically solved using Point Successive Over Relaxation (PSOR) algorithm. As seen in Eqs. (35)–(38), the vorticity and stream function, Eqs. (35) and (36), are independent from the energy and concentration equations, Eqs. (37) and (38). In order to reduce the computational time, first the vorticity-stream function was solely solved. Then, the energy and concentration equations were solved. The convective terms are discretized using upwind scheme. The numerical results are checked to assure reliably grid independent. In this way, the number of grid nodes was increased until the solution shows insignificant change by increasing the number of grid nodes.

When the maximum values of the normalized absolute residuals across all nodes are less than 10^{-10}, the iterative solution is considered to be converged. The smallest value of relaxation parameter, which is considered for convergence, for the velocity equation is 0.9 and for the temperature and concentration equations is 0.65.

4. Result and discussion

The governing equations are solved for different values of non-dimensional parameters, *Pr*, *Sc*, *Nb*, *Nt* and *Nc*. The effects of non-dimensional parameters such as *Pr*, *Sc*, *Nb*, *Nt* and *Nc* on the critical Reynolds Number at the end of the sheet (i.e. $x = 1$), and also the effects of these parameters on the fluid flow and heat transfer of nanofluid as well as reduced Nusselt and Sherwood numbers near the slit are examined. The critical Reynolds Numbers, which distinguish the non-similar region from the self-similar region, for the velocity and temperature profiles are carried out at each x and for selected presents of errors.

In order to perform a realistic analysis on the effect of non-dimensional parameters on the boundary layer, the practical range of nanofluid parameters should be analyzed [37,38]. For the water base nanofluids at room temperature with nanoparticles of 100 nm diameters, the Brownian diffusion coefficient (DB) as well as the thermophoresis coefficient (DT) ranges from 1×10^{-10} to 1×10^{-12} [36–38]. By substituting above values and thermophysical properties of common base fluids and nanoparticles in Eqs. (24) and (25), the practical ranges of these parameters is obtained. The results shows that the Schmidt number ranges from 1×10^3 to 1×10^6 and Brownian motion and thermophoresis parameters ranges from 1×10^{-9} to 1×10^{-4}.

Khan and Pop [22] and Noghrehabadi et al. [27] examined the boundary layer heat and mass transfer of nanofluids over a stretching sheet using similarity solution. The previous studies [22,27] selected the non-dimensional parameters of Prandtl number, Schmidt number, Brownian motion and thermophoresis parameters in the range of $1 < Pr < 15$, $5 < Sc < 25$, $0.1 < Nb < 0.5$ and $0.1 < Nt < 0.5$, respectively. The similarity equations can be found in Eqs. (8)–(10) in the work of Khan and Pop [22]. We need the solution of similarity equations for any combination of non-dimensional parameters. Therefore, in the present study the similarity equations, proposed by Khan and Pop [22], are solved numerically using the Rung-Kutta forth order and Newton–Raphson methods

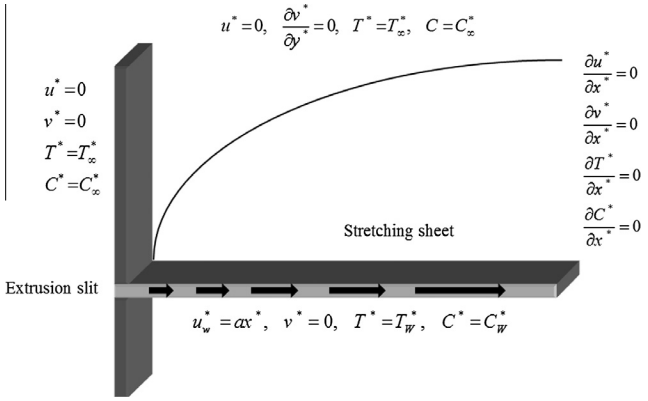

Fig. 1. Physical model and boundary conditions.

with a systematic guessing of $f''(0)$, $\theta'(0)$ and $\varphi'(0)$ by the shooting technique. It is worth noticing that $f''(0)$, $\theta'(0)$ and $\varphi'(0)$ are non-dimensional similarity variables of velocity, temperature and concentration gradients at the surface. The results of similarity solution in the present study are compared with the results reported by Khan and Pop [22] and Noghrehabadi et al. [27] in Figs. 2 and 3.

In order to verify the validity and the accuracy of the finite difference code, the results of PSOR method for the velocity, temperature and nanoparticles concentration profiles as well as the reduced Nusselt and Sherwood numbers far enough from the extrusion slit are compared with the results in the self-similar region which is obtained by similarity solution and those results reported by Khan and Pop [22] and Noghrehabadi et al. [27]. Tables 1 and 2 show a comparison between the results of similarity solution and PSOR method (with selected grid size) and the results which carried out by Khan and Pop [15]. According to results of these tables, the grid sizes 50×100, 50×300 are appropriate for numerical calculations. Hence, the grid size of 50×300 is selected to ensure the accuracy of the solution for different combination of non-dimensional parameters. 50×300 indicates 50 grid points along the x-axis and 300 grid points along the y-axis.

Fig. 2 illustrates the effects of Reynolds number on the velocity profiles. As seen, an increase of Reynolds number would

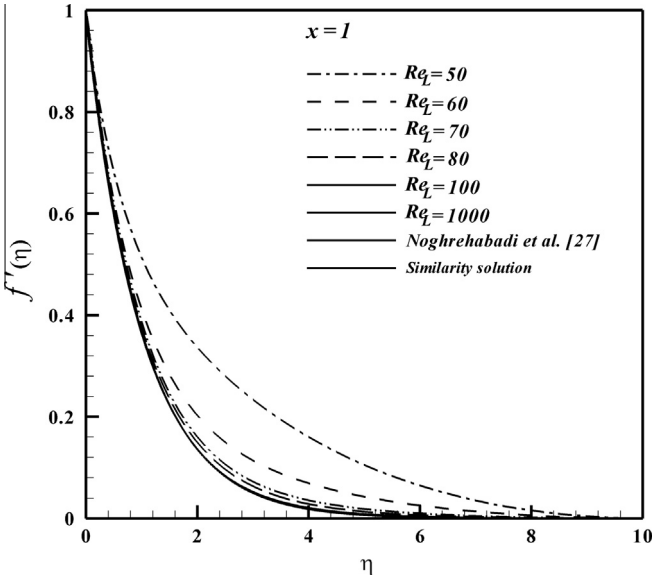

Fig. 2. Effects of Re_L number on the velocity profile and comparisons with Noghrehabadi et al. [27].

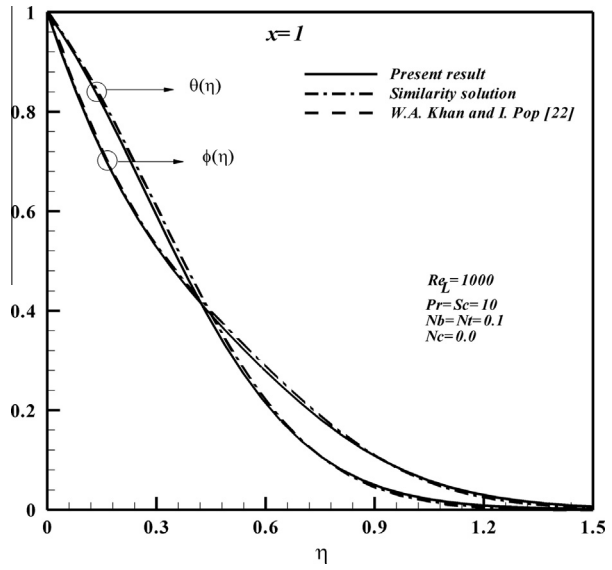

Fig. 3. Comparisons between the current results and the results that reported by Khan and Pop [22] for temperature and concentration profiles.

decreases the velocity profiles in the boundary layer. Moreover, for $Re_L \geqslant 100$, when $x = 1$, velocity profiles unify on one curve that means, $Re_L \approx 100$ is a critical Reynolds number to specify the non-similar region from self-similar region of velocity profiles. In addition, the velocity profiles in the self-similar region are compared with the results of similarity solution and those reported by Noghrehabadi et al. [27].

Fig. 3 shows a comparison between the temperature and concentration profiles at the end of the sheet, obtained in the present study and those reported by Khan and Pop [22]. Fig. 3 clearly depicts that when the Prandtl, Brownian motion, thermophoresis and Schmidt numbers take constant values, the results at the end of the sheet, i.e. $x = 1$, are very similar to those of Khan and Pop [22].

The PSOR results of Tables 1 and 2 and Figs. 2 and 3 regarding to the self-similar region, show very good agreement with the results of similarity solution and the results reported by previous studies [22] and [27].

Fig. 4 shows the values of critical Reynolds numbers of hydrodynamic boundary layer as function of x for selected values of error percent. Fig. 4 reveals that the velocity profiles in the whole domain of the boundary layer are in the self-similar region with less than 5% error when $Re_L \geqslant 94$. The results of Fig. 4 can be directly utilized to show the boundary of self-similar region. For example, assuming a practical case with $\upsilon = 10^{-5}$ (m^2/s), $aL = 0.01$ (m/s) and $L = 0.1$ (m), Reynolds number is equal to 100, which means the velocity profile is in self-similar domain for every length of the sheet (x) with less than 5% error; in the same situation, when

Table 2
The values of reduced Sherwood number *Shr* at the end of the sheet $x = 1$, when $\beta_x = 2.0$, $\beta_y = 1.01$, $Sc = Pr = 10$ and $Re_L = 1000$.

	Nb = 0.1				
	Nt = 0.1	Nt = 0.2	Nt = 0.3	Nt = 0.4	Nt = 0.5
Khan and Pop [22]	2.1294	2.2740	2.5286	2.7952	3.0351
Similarity solution	2.129395	2.274021	2.528636	2.795166	3.035143
PSOR 50 × 100	2.118090	2.248390	2.495599	2.761388	3.005559
Error% 50 × 100	0.5	1.1	1.3	1.2	1.0
PSOR 50 × 200	2.122728	2.259689	2.510216	2.775991	3.017920
Error% 50 × 200	0.3	0.6	0.7	0.7	0.6
PSOR 50 × 300	2.123178	2.261983	2.513108	2.778642	3.018960
Error% 50 × 300	0.3	0.5	0.6	0.6	0.5

$x = 0.5$ the critical Reynolds number is almost equivalent to 50 which show there is about 20% error between similarity solution and full solution of governing equations (PSOR).

Fig. 5 shows the effects of Reynolds number on the reduced skin friction coefficient. It is found that increasing the Reynolds number from 100 to 250 would decrease the values of the reduced skin friction coefficient, however, increasing the Reynolds number from 250 to 1000 does not significantly affect the reduced skin friction coefficient. For Reynolds number larger than 250 the values of *Cfr* become close to −2, which is the result of the reduced skin friction coefficient of similarity solution.

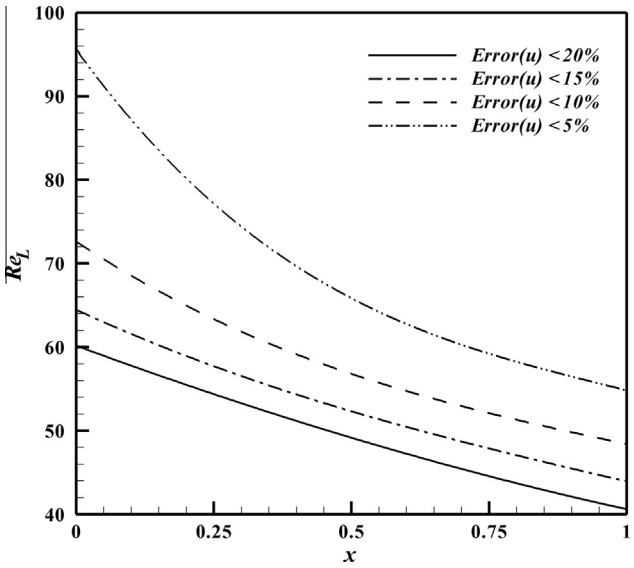

Fig. 4. The critical Reynolds number for velocity profile in each x for different values of error.

Table 1
The values of reduced Nusselt number *Nur* at the end of the sheet $x = 1$, when $\beta_x = 2.0$, $\beta_y = 1.01$, $Sc = Pr = 10$ and $Re_L = 1000$.

	Nb = 0.1				
	Nt = 0.1	Nt = 0.2	Nt = 0.3	Nt = 0.4	Nt = 0.5
Khan and Pop [22]	0.9524	0.6932	0.5201	0.4026	0.3211
Similarity solution	0.952376	0.693174	0.520079	0.402581	0.321054
PSOR 50 × 100	0.980001	0.719430	0.543927	0.423719	0.339601
Error% 50 × 100	2.9	3.8	4.6	5.3	5.8
PSOR 50 × 200	0.966613	0.706702	0.532372	0.413524	0.330658
Error% 50 × 200	1.5	2.0	2.36	2.7	3.0
PSOR 50 × 300	0.962820	0.702998	0.529042	0.4105583	0.328182
Error% 50 × 300	1.1	1.4	1.7	2.0	2.2

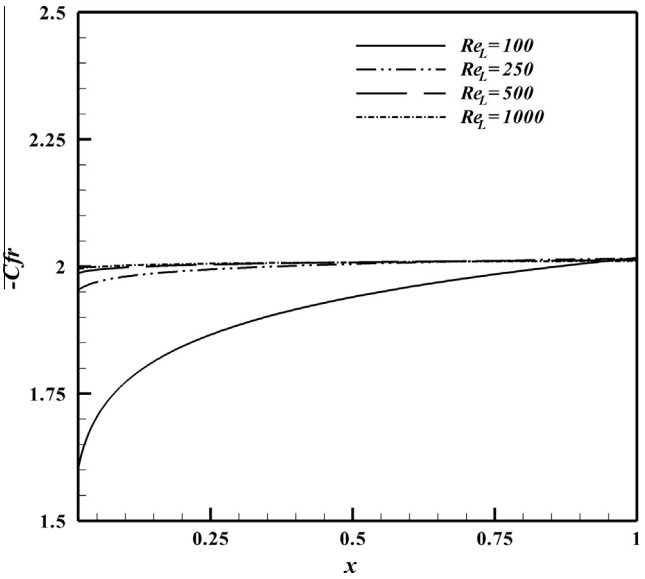

Fig. 5. Effects of Re_L number on the reduced skin friction coefficient.

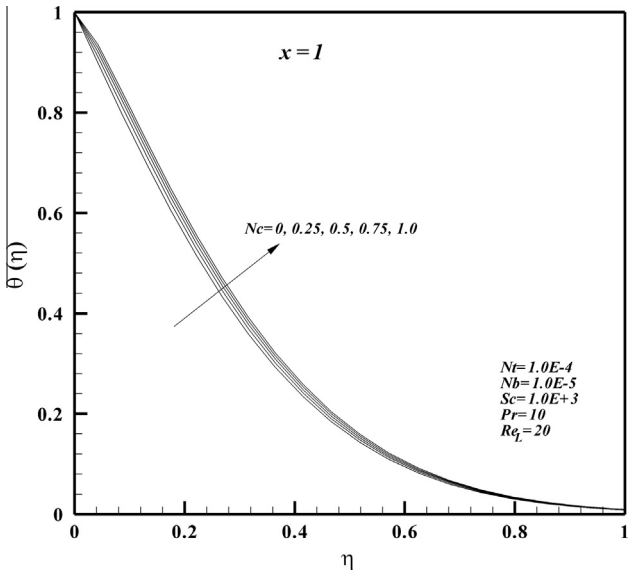

Fig. 7. Effects of variable thermal conductivity *Nc* on the temperature profile.

Fig. 6 illustrates the effects of Prandtl number on the temperature profiles for various values of Reynolds number. Obviously, the temperature profiles overlap on one curve when $x = 1$ and Reynolds number $Re_L \geqslant 50$. Therefore, it can be concluded that $Re_L \approx 50$ is the critical Reynolds number for the temperature profiles (in the case of $Pr = 5$). In addition, it is clear that an augmentation of Prandtl number would reduce the critical Reynolds number. For example, the critical Reynolds number is about 50 when $Pr = 5$, and it is about 20 when $Pr = 15$. The same trend of behavior was reported previously by Al-Sanea and Ali [6] and Kiwan and Ali [7] in the case of pure fluid.

The effect of variable thermal conductivity parameter on the temperature profiles are depicted in Fig. 7. Obviously, an increase of the variable thermal conductivity would increase the thickness of thermal boundary layer. A reason for this behavior is that an increase of *Nc* would increase the thermal conductivity of the nanofluid in the vicinity of the wall where the local concentration of nanoparticles is comparatively high; thereby, the temperature profiles would increase.

The values of critical Reynolds number for temperature profiles at each *x* are illustrated in Fig. 8. This figure reveals that the most of the sheet length is in the self-similar region when $Re_L \approx 50$ and $Pr = 5$ within the error of less than 5%. In addition, an increase of the Prandtl number would decrease the critical Reynolds number which is in good agreement with the results of Fig. 6. It is worth noticing that the temperature profiles in the whole domain of the boundary layer would change to the self-similar region for comparatively high values of Reynolds number. Therefore, as seen in Fig. 8, the boundary layer approximation, at the beginning of the sheet ($0 < x < 0.034$), is not valid for a large ranges of Reynolds number ($Re_L < 2600$) when $Pr = 5$.

The values of reduced Nusselt number for different values of Reynolds number, Prandtl number and variable thermal conductivity parameters are displayed in Figs. 9–11. It can be observed that

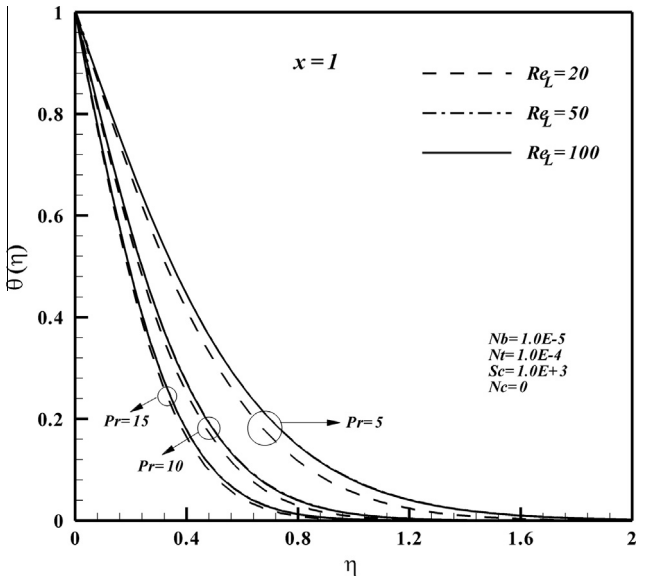

Fig. 6. Effects of Re_L number and Prandtl number *Pr* on the temperature profile.

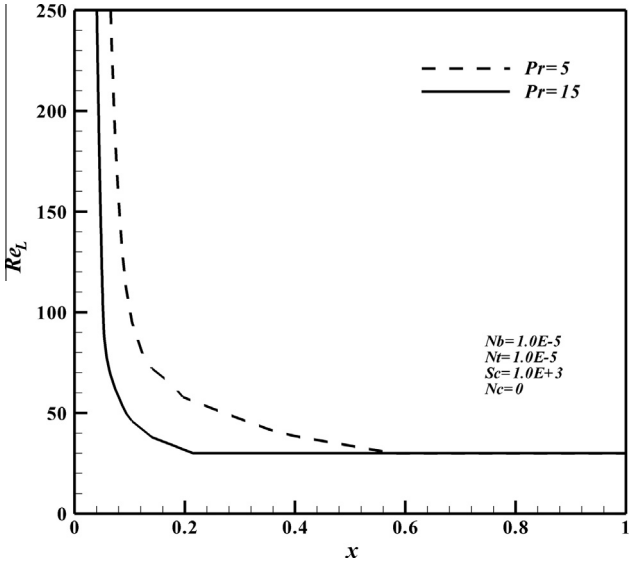

Fig. 8. The critical Reynolds number for temperature profile in each *x* when error <5%.

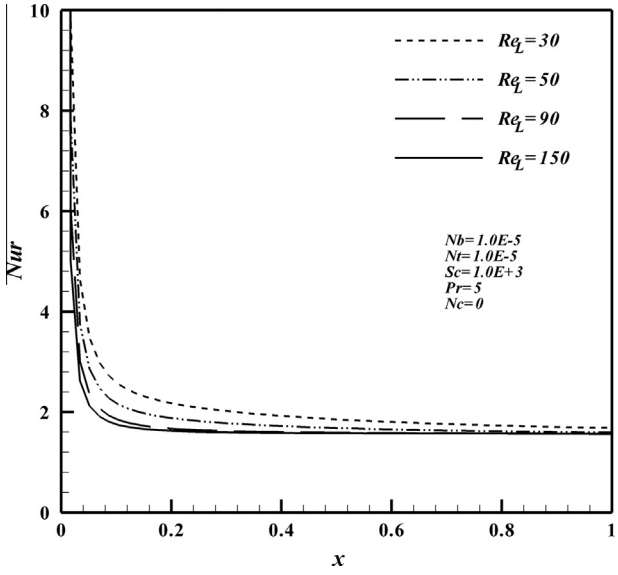

Fig. 9. Effects of Reynolds number Re_L on the reduced Nusselt number *Nur*.

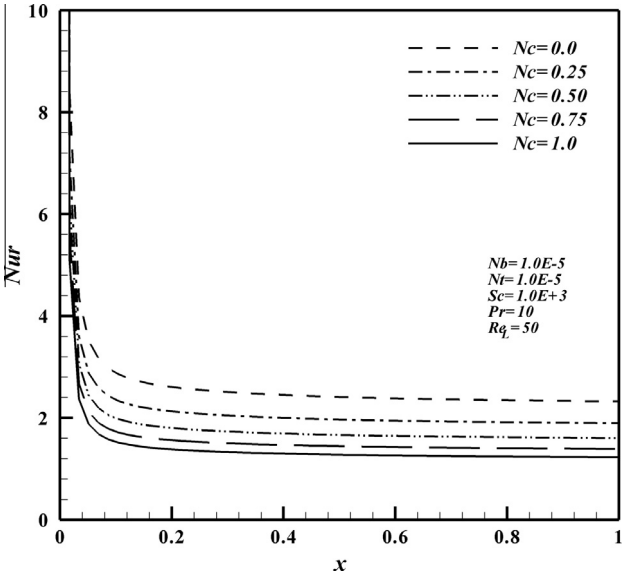

Fig. 11. Effects of variable thermal conductivity parameter *Nc* on the reduced Nusselt number *Nur*.

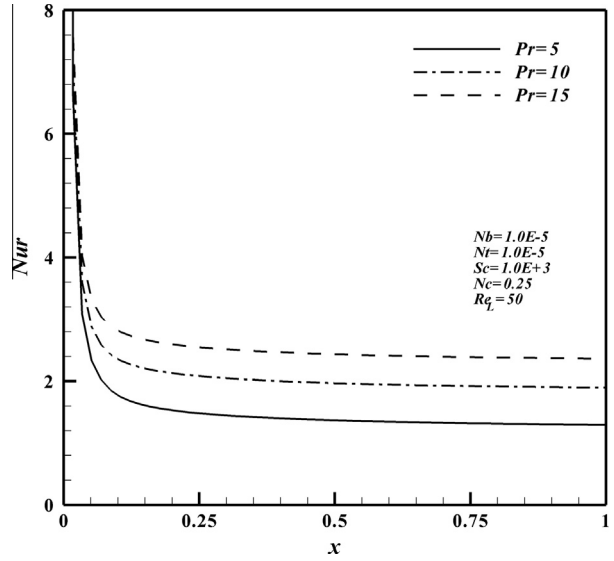

Fig. 10. Effects of Prandtl number *Pr* on the reduced Nusselt number *Nur*.

the reduced Nusselt number is a decreasing function of Reynolds number and variable thermal conductivity parameter; however, it is an increasing function of Prandtl number. The same conclusion for the effects of Prandtl number on the reduced Nusselt number in the self-similar region was reported in works by Khan and Pop [22] and Hassani et al. [23]. These figures show that the values of reduced Nusselt numbers at the end of the sheet tend to converge to the values of reduced Nusselt number obtained by the similarity solution. It is worth noticing that the reduced Nusselt number obtained by the similarity solution (when $Nb = Nt = 1.0E{-}5$, $Sc = 1000$ and $Pr = 5$) is equal to 1.57 while the results of Fig. 9 demonstrate that the values of reduced Nusselt number at the end of the sheet (i.e. $x = 1$) for $Re_L = 30, 50, 90, 150$ are respectively equal to 1.69, 1.59, 1.57, 1.57. Therefore, it can be concluded that at the end of the sheet the values of the reduced Nusselt number when $Re_L \geqslant 50$ are very close to the values of self-similar region. However, at the beginning of the sheet, the values of the reduce Nusselt number are very far from the values of self-similar region.

For example when $Nb = Nt = 1.0E{-}5$, $Sc = 1000$ and $Pr = 5$, the reduced Nusselt number is equal to 314 for the range of Reynolds number between 30 and 150. The same trend of the results was observed in Fig. 8 for the temperature profiles.

Figs. 12 and 13 show the effects of Reynolds and Schmidt number on the reduced Sherwood number. The reduced Sherwood number is a decreasing function of Reynolds number while it is an increasing function of Schmidt number. Schmidt number (υ/DB) shows the ratio of the diffusion of viscosity and the diffusion of nanoparticles. Increasing the Schmidt number would increase the convection of the nanoparticles along the boundary layer. Hence, mass transfer is an increasing function of Schmidt number. Previously, the same conclusion was reported by Khan and Pop [22] and Hassani et al. [23] for the effects of Schmidt number on the reduced Sherwood number in the self-similar region. It is worth noticing that the values of the reduced Sherwood number at the end of the sheet (i.e. $x = 1$) when $Re_L \geqslant 50$ are very close to

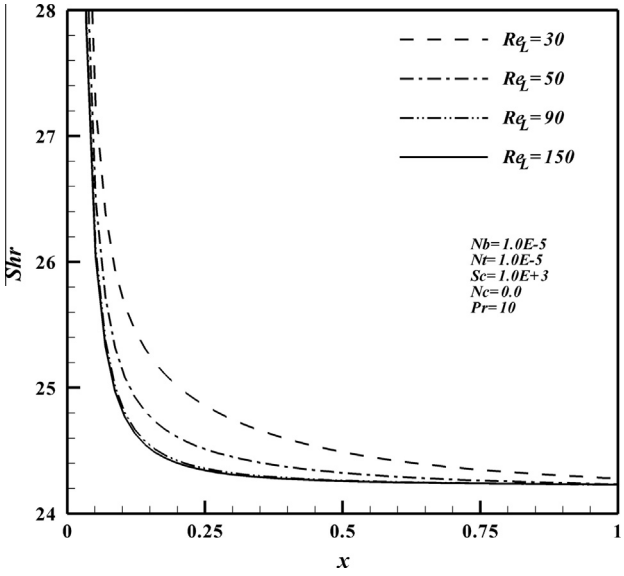

Fig. 12. Effects of Reynolds number Re_L on the reduced Sherwood number *Shr*.

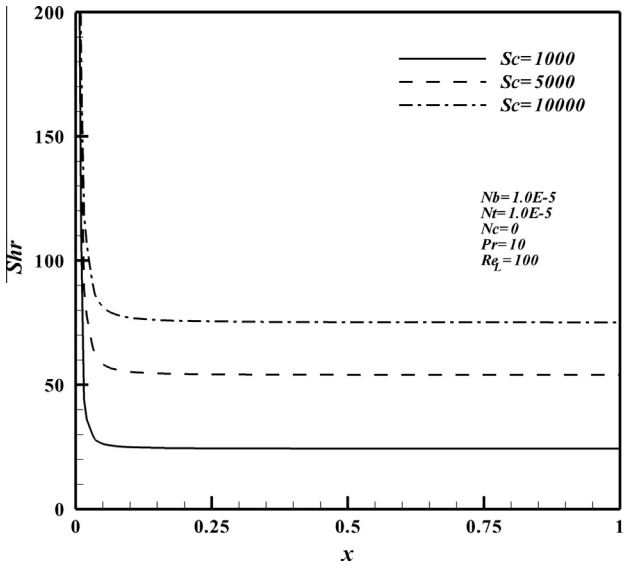

Fig. 13. Effects of Schmidt number *Sc* on the reduced Sherwood number *Shr*.

the values of self-similar region. In addition, it can be seen from Fig. 12, for $Re_L \geqslant 90$, the Sherwood number for $x > 0.25$ become close to 24 which shows the value of the Sherwood number for self-similar region. As an example, considering a nanofluid with $\upsilon = 10^{-5}$ (m^2/s), stretching velocity $aL = 0.001$(m/s) and sheet length $L = 1$, the Reynolds number is equal to 100 which can be concluded, the mass transfer (*Shr*) from the beginning of the sheet $x = 0$ to $x = 0.25$ is not in the self-similar region.

The effects of Brownian motion and thermophoresis parameters in practical ranges (1×10^{-9} to 1×10^{-4}) on the critical Reynolds number are also investigated. However, because the values of Brownian motion and thermophoresis are small, these effects can be neglected and the results are not presented here to conserve space. In addition, the variable thermal conductivity increase the thickness of the thermal boundary layer but it has not any effect on the critical Reynolds number.

5. Conclusion

The boundary layer flow and heat transfer of nanofluids over a stretching sheet near the extrusion slit is investigated numerically using the finite difference scheme and PSOR algorithm. The governing partial differential equations, which incorporate the effects of Brownian motion and thermophoresis, were transformed to the dimensionless form. A critical Reynolds number, which distinguishes the non-similar region from the self-similar region, is introduces. Moreover, the effects of dimensionless parameters namely Prandtl namber *Pr*, Schmidt number *Sc*, variable thermal conductivity parameter *Nc*, Brownian motion number *Nb* and thermophoresis parameter *Nt* on the thermal boundary layer, reduced Nusselt and Sherwood numbers and critical Reynolds number $Re_{L,C}$ are analyzed. The most important findings of the present study can be summarized as follows:

- The critical Reynolds number for the velocity profiles is $Re_{L,C} = 94$. For $Re_L \geqslant 94$ the whole domain of velocity profile has less than 5% error compared to the results of similarity solution.
- It is found that the temperature profiles in the most parts of the sheet are in the self-similar region when $Re_{L,C} \approx 50$ and $Pr = 5$ with less than 5% error. However, the temperature profiles for the whole domain, change to self-similar region in very high Reynolds number. In addition, Prandtl number significantly affects the critical Reynolds number for temperature profile.
- An increasing of the variable thermal conductivity parameter would increase the thickness of the thermal boundary layer.
- The reduced Nusselt *Nur* and reduced Sherwood *Shr* numbers near the extrusion slit are much higher than those downstream from the extrusion slit. Moreover, the reduced Nusselt *Nur* and reduced Sherwood *Shr* numbers are a decreasing function of Reynolds number; however they are an increasing function of Prandtl and Schmidt numbers, respectively.

References

[1] Tadmor Z, Klein I. Engineering principles of plasticating extrusion. Van Nostrand Reinhold; 1970.
[2] Fisher EG. Extrusion of plastics. Wiley; 1976.
[3] Sakiadis BC. Boundary layer behavior on continuous solid surfaces: I. Boundary layer equations for two dimensional and axisymmetric flow. AIChE J 1961;7:26–8.
[4] Sakiadis BC. Boundary layer behavior on continuous solid surfaces: II. Boundary layer on a continuous flat surface. AIChE J 1961;7:221–5.
[5] Crane LJ. Flow past a stretching plate. ZAMP 1970;21:645–7.
[6] Al-Sanea SA, Ali ME. The effect of extrusion slit on the flow and heat-transfer characteristics from a continuously moving material with suction or injection. Int J Heat Fl 2000;21:84–91.
[7] Kiwan S, Ali ME. Near-slit effects on the flow and heat transfer from a stretching plate in a porous medium. Numer Heat Tr A – Appl 2008;54:93–108.
[8] Choi SUS. Enhancing thermal conductivity of fluids with nanoparticle. In: Siginer DA, Wang HP, editors. Developments and applications of non-newtonian flows, FED vol. 231 and MD vol. 66. ASME; 1995. p. 99–105.
[9] Masuda H, Ebata A, Teramea K, Hishinuma N. Altering the thermal conductivity and viscosity of liquid by dispersing ultra-fine particles. Netsu Bussei 1993;4:227–33.
[10] Das SK, Choi SUS, Yu W, Pradeep T. Nanofluids – science and technology. Hoboken: John Wiley & Sons Publishers; 2007.
[11] Wang XQ, Mujumdar AS. A review on nanofluids – Part I: Theoretical and numerical investigations. Braz J Chem Eng 2008;25:613–30.
[12] Kakaç S, Pramuanjaroenkij A. Review of convective heat transfer enhancement with nanofluids. Int J Heat Mass Trans 2009;52:3187–96.
[13] Chandrasekar M, Suresh S, Senthilkumar T. Mechanisms proposed through experimental investigations on thermophysical properties and forced convective heat transfer characteristics of various nanofluids – a review. Renew Sust Energy Rev 2012;16:3917–38.
[14] Wu JM, Zhao J. A review of nanofluid heat transfer and critical heat flux enhancement-Research gap to engineering application. Prog Nucl Energy 2013;66:13–24.
[15] Olanrewaju AM, Makinde OD. On boundary layer stagnation point flow of a nanofluid over a permeable flat surface with Newtonian heating. Chem Eng Commun 2013;200:836–52.
[16] Ibrahim W, Makinde OD. The effect of double stratification on boundary-layer flow and heat transfer of nanofluid over a vertical plate. Comput Fluids 2013;86:433–41.
[17] Mutuku WN, Makinde OD. Hydromagnetic bioconvection of nanofluid over a permeable vertical plate due to gyrotactic microorganisms. Comput Fluids 2014.
[18] Njane M, Mutuku WN, Makinde OD. Combined effect of Buoyancy force and Navier slip on MHD flow of a nanofluid over a convectively heated vertical porous plate. Sci World J 2013.
[19] Makinde OD. Computational modelling of nanofluids flow over a convectively heated unsteady stretching sheet. Curr Nanosci 2013;9:673–8.
[20] Makinde OD. Effects of viscous dissipation and Newtonian heating on boundary-layer flow of nanofluids over a flat plate. Int J Numer Methods Heat Fluid Flow 2013;23:1291–303.
[21] Makinde OD, Khan WA, Aziz A. On inherent irreversibility in Sakiadis flow of nanofluids. Int J Exergy 2013;13:159–74.
[22] Khan WA, Pop I. Boundary-layer flow of a nanofluid past a stretching sheet. Int J Heat Mass Trans 2010;53:2477–83.
[23] Hassani M, Tabar MM, Nemati H, Domairry G, Noori F. An analytical solution for boundary layer flow of a nanofluid past a stretching sheet. Int J Therm Sci 2011;50:2256–63.
[24] Kahar RA, Kandasamy R, Muhaimin. Scaling group transformation for boundary-layer flow of a nanofluid past a porous vertical stretching surface in the presence of chemical reaction with heat radiation. Comput Fluids 2011;52:15–21.
[25] Makinde OD, Aziz A. Boundary layer flow of a nanofluid past a stretching sheet with a convective boundary condition. Int J Therm Sci 2011;50:1326–32.
[26] Rana P, Bhargava R. Flow and heat transfer of a nanofluid over a nonlinearly stretching sheet: a numerical study. Commun Nonlinear Sci Numer Simul 2012;17:212–26.
[27] Noghrehabadi A, Pourrajab R, Ghalambaz M. Effect of partial slip boundary condition on the flow and heat transfer of nanofluids past stretching sheet prescribed constant wall temperature. Int J Therm Sci 2012;54:253–61.

[28] Noghrehabadadi A, Ghalambaz M, Ghanbarzadeh A. Heat transfer of magnetohydrodynamic viscous nanofluids over an isothermal stretching sheet. J Thermophys Heat Transfer 2012;26:686–9.
[29] Noghrehabadi A, Pourrajab R, Ghalambaz M. Flow and heat transfer of nanofluids over stretching sheet taking into account partial slip and thermal convective boundary conditions. Heat Mass Transfer 2013;49:1357–66.
[30] Noghrehabadi A, Saffarian M, Pourrajab M, Ghalambaz M. Entropy analysis for nanofluid flow over a stretching sheet in the presence of heat generation/absorption and partial slip. J Mech Sci Technol 2013;27:927–37.
[31] Ibrahim W, Shankar B. MHD boundary layer flow and heat transfer of a nanofluid past a permeable stretching sheet with velocity, thermal and solutal slip boundary conditions. Comput Fluids 2013;75:1–10.
[32] Nadeem S, Mehmood R, Akbar NS. Non-orthogonal stagnation point flow of a nano non-Newtonian fluid towards a stretching surface with heat transfer. Int J Heat Mass Transfer 2013;57:679–89.
[33] Nadeem S, Haq RU, Akbar NS, Lee C, Khan ZH. Numerical study of boundary layer flow and heat transfer of Oldroyd-B nanofluid towards a stretching sheet. PLoS ONE 2013;8.
[34] Chandrasekar M, Suresh S. A review on the mechanisms of heat transport in nanofluids. Heat Transfer Eng 2009;30:1136–50.
[35] Khanafer K, Vafai K. A critical synthesis of thermophysical characteristics of Nanofluids. Int J Heat Mass Transfer 2011;54:4410–28.
[36] Buongiorno J. Convective transport in nanofluids. J Heat Trans-T ASME 2006;128:240–50.
[37] Noghrehabadi A, Ghalambaz M, Ghanbarzadeh A. Effects of variable viscosity and thermal conductivity on natural-convection of nanofluids past a vertical plate in porous media. J Mech 2013:1–11. http://dx.doi.org/10.1017/jmech.2013.61.
[38] Noghrehabadi A, Behseresht A. Flow and heat transfer affected by variable properties of nanofluids in natural-convection over a vertical cone in porous media. Comput Fluids 2013;88:313–25.